

Brownian dynamics of Dirac fermions in twisted bilayer graphene

Abdullah Yar*¹

¹*Department of Physics, Kohat University of Science and Technology,
Kohat 26000, Khyber Pakhtunkhwa, Pakistan**

Brownian dynamics of Dirac fermions in twisted bilayer graphene is investigated within the framework of semiclassical relativistic Langevin equations. We find that under the influence of orthogonal, commensurate ac drives in the periodic ratchet potential of a substrate, the charge carriers in the system exhibit pronounced random dynamics, tuned by the twist angle, making twisted bilayer graphene distinguishable from monolayer graphene. It is shown that as threshold twist angle matches the optimal angle, deterministic running states appear in the limit of weak thermal noise where the diffusion rate is enhanced significantly compared to bare thermal diffusion. Analysis of the real space trajectories and diffusion coefficient illustrates the significant role of thermal noise in the random motion of Dirac fermions. In addition, we find that the Brownian particle shows remarkable ratchet effect as a net current.

I. INTRODUCTION

The study of exotic properties of twisted bilayer graphene (TBG) has attracted significant attention in condensed matter physics [1–8]. It is composed of two monolayer graphene sheets, obtained by stacking one layer of graphene on top of another and rotating the two layers by a small twist angle, leading to a moiré pattern to arise between the lattices of the two graphene layers. It can be realized as a model platform for investigating the properties of semiconducting flat band moiré van der Waals heterostructures. It has been found that the Dirac crossings in TBG are protected by the product of two-fold rotational and time-reversal symmetries (C_2T) [9]. A long period moiré pattern is formed if stacking of the two graphene monolayers is slightly disoriented, leading to a significant reduction of Fermi velocity at the Dirac cone. In TBG, the concentration of charge density is maximal around a moiré pattern, leading to the formation of a triangular lattice structure [10–14]. The quantum states of Dirac fermions in the vicinity of each valley of graphene sheet hybridize with the electronic states of the other sheet, resulting into interesting electronic band structure. It has been shown that two nearly flat bands are formed in the middle of the full energy band, separated from other energy bands for the twisting angle being close to magic angles [15]. The interaction effects are very enhanced when the chemical potential remains inside these nearly flat bands. Remarkable unconventional superconducting phases [2] and Mott insulator behavior [1] have been observed in the transport studied of TBG. Interesting dissipation processes [16–19], temperature-dependent electrical transport [20], tunable large Berry curvature [21], nonlinear Hall effect [22], carrier confinement [23], and topological Hofstadter butterfly [24] have been investigated in TBG. The flat bands in twisted bilayer graphene have been observed experimentally using local tunnelling spec-

troscopy technique [10, 25–28], electronic compressibility measurements [29], and direct momentum-resolved measurements [30]. Another possible method for detecting flat bands in TBG is the combination of different imaging techniques with angle-resolved photoemission spectroscopy (ARPES) that can be used to observe the flat band structures in twisted bilayer graphene devices [31]. On the other hand, the study of Brownian motion has been the focus of active research [32]. It is the description of any physical phenomenon in which some quantities are constantly undergoing small random fluctuations. It also provides insights into the numerical solution of stochastic differential equations. The Brownian particle experiences irregular forces as a result of random collisions with atoms or molecules of the medium, which alter both the direction and magnitude of the velocity of charge carrier. The study of Brownian motion has played an important role in the development of both the foundations of thermodynamics and the dynamical interpretation of statistical physics. The theory of Brownian motion based on molecular-kinetic theory of heat provides the link between an elementary underlying microscopic dynamics and macroscopic observable phenomena. It has been shown that a particle undergoes a zero-temperature localization-delocalization transition in a periodic potential with the decrease of dissipation strength [33]. Moreover, optimal estimation of diffusion coefficient of a diffusing particle from a single-time-lapse recorded trajectory of the particle has been studied [34]. Likewise, periodically driven Brownian motion of a massive particle in one dimension subjected to dry friction has been investigated [35]. Recently, non-random dynamics of DNA molecules in the regime where length scales are greater than the size of molecule, undetectable by the analysis of mean squared displacement (MSD), a measure of the deviation of the position of a particle with respect to a reference position, has been quantified by characterizing the molecular motion relative to a latticed frame of reference [36]. Moreover, other interesting aspects of Brownian motion have been studied. For instance, active random motion with intermittent direction reversals [37], nanoparticle dynamics in nanofluid [38], highly resolved

* abdullahyardawar@gmail.com

random motion in space and time [39], Brownian behavior in coupled chaotic oscillators [40], paradigmatic model of Brownian motion in a harmonic oscillator coupled to a bath of oscillators [41], Brownian motion in a Landau level system [42] have been reported.

It has been shown that a driven Brownian dynamics is described by two states: (i) locked state, where the Brownian particle resides inside one potential well, which is obtained in the limit of small driving force strength. (ii) Running state in which the particle runs over the potential barriers, which appears in the large driving force strength regime. In these regions, both the diffusion and regular behaviours of the Brownian particle are accessible. Brownian dynamics can be characterized by the standards: (i) availability of noise, where the interplay among nonlinearity, noise-mediated dynamics, and non-equilibrium driving leads to an unpredictable electronic transport. (ii) Temporal periodically driven supplemented symmetry breaking, usually involved in the periodically operating devices.

In view of the promising characteristic features exhibited by the Dirac fermions, we report the Brownian dynamics in twisted bilayer graphene (TBG). It has been found that Dirac fermions in TBG show transport properties different from monolayer graphene, for instance, the TBG exhibit finite nonlinear Hall effect [22] which vanishes in monolayer graphene.

In this work, we show that the Dirac fermions in TBG exhibit pronounced Brownian motion, tuned by the twist angle, presenting transport scenario different from monolayer graphene. In addition, we investigate ratchet effect as a net current. The investigation of Brownian dynamics in TBG may be an interesting aspect of dynamics with the possible experimental observation.

The paper is organized as follows: Methodology for the Brownian dynamics of Dirac fermions in twisted bilayer graphene is presented in Sec. II. The band structure of TBG is determined, followed by the description of relativistic semiclassical Langevin equations. In Sec. III, results and discussion are presented with the evaluation and analysis of diffusion coefficient as a function of thermal noise, ratchet potential strength, driving force field amplitude, and twist angle. Ratcheting as a net current is also demonstrated in this section. Finally, the summary of results is presented in Sec. IV.

II. METHODOLOGY

In this section, we present the detailed methodology of the diffusion mechanism in TBG driven by orthogonal, commensurate ac drives in a periodic ratchet potential of a substrate.

A. Model Hamiltonian

We consider a hexagonal-lattice model that reflects the symmetry properties and number of subbands of the flat band in twisted bilayer graphene (TBG). Taking into account the nearest neighbor hopping, the tight-binding Hamiltonian within the continuum model approach can be expressed as [43]

$$\mathcal{H}_0(\mathbf{k}) = \begin{pmatrix} 0 & h_{\mathbf{k}} \\ h_{\mathbf{k}}^* & 0 \end{pmatrix}, \quad (1)$$

with

$$h_{\mathbf{k}} = \frac{W}{3} \sum_{\delta_l} e^{i\mathbf{k}\cdot\delta_l}, \quad (2)$$

where $W/3$ represents the hopping matrix element to nearest neighbours at positions $\delta_l = (\cos(2\pi l/3), \sin(2\pi l/3)) L_M/\sqrt{3}$, where $l = 0, 1, 2$ and L_M is the moiré superlattice periodicity, realized in twisted bilayer graphene. It is illustrated that W represents the bandwidth measured from Dirac point, and the nearest neighbour distance $L_M/\sqrt{3}$ is chosen such that the lattice period of the hexagonal model mimics the moiré superlattice period. Following the analysis of Lewandowski and Levitov [43], we choose the energy and length scales such as the width of a single band W and the hexagonal lattice period L_M to be identical to the parameters in TBG: $W = 3.75\text{meV}$ and $L_M = a/2 \sin(\theta/2)$ is the moiré superlattice period, yielding $L_M = 13.4\text{nm}$ for the magic angle $\theta = 1.05^\circ$ and lattice constant of graphene, $a = 0.246\text{nm}$. The relativistic energy dispersion of the Dirac fermions is

$$E_\lambda(\mathbf{k}) = \lambda|h_{\mathbf{k}}|, \quad (3)$$

where $\lambda = \pm$ is the band index and $|h_{\mathbf{k}}| = \frac{W}{3} \sqrt{1 + 4 \cos\left(\frac{L_M}{2} k_y\right) \cos\left(\frac{\sqrt{3}L_M}{2} k_x\right) + 4 \cos^2\left(\frac{L_M}{2} k_y\right)}$. In the following analysis, we use Eq. (3) with $\lambda = +$.

B. Relativistic Langevin equations

We consider a sample of twisted bilayer graphene (TBG) on a substrate with a periodic potential $V(x)$. TBG is driven by two orthogonal harmonic drives $E_x(t)$ and $E_y(t)$ with commensurate frequencies, inducing rectification that leads to a direct current. The ratchet substrate in one dimension is modeled by the double-sine potential as [32, 44–46]

$$V(x) = V_0 \left[\sin\left(\frac{2\pi x}{L}\right) + \mu \sin\left(\frac{4\pi x}{L}\right) \right], \quad (4)$$

where V_0 is the strength, L is the period of the potential, and $\mu = 1/4$ is a constant. The Brownian motion of

Dirac fermions in TBG can be described by a set of coupled relativistic Langevin equations for the components of 2D momentum, $\mathbf{k} = (k_x, k_y)$, subjected to the relativistic dispersion relation given in Eq. (3). These equations are determined by the condition that the chosen particle-reservoir coupling must lead to the same equilibrium momentum distribution as predicted by the fully microscopic theory. We follow the procedure of Dunkel *et al.* [47] and Pototsky *et al.* [44] for deriving the coupled relativistic Langevin equations. For describing the random dynamics, charge carriers in TBG require high energies for their distribution to be appropriately approximated by the relativistic Jüttner distribution,

$$f(\mathbf{k}) \sim \exp[-E(\mathbf{k})/k_B T]. \quad (5)$$

For a technical discussion on validity of the relativistic Jüttner distribution, the relevant approximations and detailed derivations of the coupled relativistic Langevin equations, the reader is referred to Refs. [44, 47]. Here we emphasize that the Jüttner distribution can be regarded as a semiclassical approximation of the Fermi-Dirac distribution for relativistic particles with rest energy on the order of, or smaller than $k_B T$. Such a condition is valid for charge carriers in TBG in the vicinity of Dirac points. In cartesian coordinates, a convenient [44] but not unique [47] set of semiclassical coupled relativistic Langevin equations consistent with the above 2D relativistic Jüttner distribution is

$$\dot{x} = \frac{1}{\hbar} \frac{\partial |h_{\mathbf{k}}|}{\partial k_x}, \quad (6)$$

$$\dot{y} = \frac{1}{\hbar} \frac{\partial |h_{\mathbf{k}}|}{\partial k_y}, \quad (7)$$

$$\dot{k}_x = -\frac{\eta}{\hbar^2} \frac{\partial |h_{\mathbf{k}}|}{\partial k_x} - \frac{1}{\hbar} \frac{dV(x)}{dx} + \frac{e}{\hbar} E_x(t) + \frac{1}{\hbar} \sqrt{2\eta k_B T} \zeta_x(t), \quad (8)$$

$$\dot{k}_y = -\frac{\eta}{\hbar^2} \frac{\partial |h_{\mathbf{k}}|}{\partial k_y} + \frac{e}{\hbar} E_y(t) + \frac{1}{\hbar} \sqrt{2\eta k_B T} \zeta_y(t), \quad (9)$$

where η is the damping constant, $E_x(t)$ and $E_y(t)$ are the driving ac electric fields in the x - and y -directions, respectively, whereas

$$\frac{\partial |h_{\mathbf{k}}|}{\partial k_x} = -\frac{WL_M}{\sqrt{3}} \times \frac{\cos\left(\frac{L_M}{2} k_y\right) \sin\left(\frac{\sqrt{3}L_M}{2} k_x\right)}{\sqrt{1 + 4 \cos\left(\frac{L_M}{2} k_y\right) \cos\left(\frac{\sqrt{3}L_M}{2} k_x\right) + 4 \cos^2\left(\frac{L_M}{2} k_y\right)}}, \quad (10)$$

and

$$\frac{\partial |h_{\mathbf{k}}|}{\partial k_y} = -\frac{WL_M}{3\hbar} \times \frac{\left[\cos\left(\frac{\sqrt{3}L_M}{2} k_x\right) \sin\left(\frac{L_M}{2} k_y\right) + \sin\left(L_M k_y\right)\right]}{\sqrt{1 + 4 \cos\left(\frac{L_M}{2} k_y\right) \cos\left(\frac{\sqrt{3}L_M}{2} k_x\right) + 4 \cos^2\left(\frac{L_M}{2} k_y\right)}}. \quad (11)$$

The random forces $\zeta_x(t)$ and $\zeta_y(t)$ in Eqs. (8) and (9) are two white Gaussian noises with vanishing mean, $\langle \zeta_m(t) \rangle = 0$, satisfying the fluctuation-dissipation relation, $\langle \zeta_m(t) \zeta_n(t_0) \rangle = \delta_{mn} \delta(t - t_0)$, with $m, n = x, y$, which ensures proper thermalization at temperature T . The damping coefficient γ contains contributions from all possible collision mechanisms including phonon scattering, a charge carrier may undergo when moving on the surface of a TI attached to SMO. In order to take into account microscopic collision mechanisms requires a detailed quantum kinetic theory, for instance, see [48], which is beyond the scope of our semi-classical approach considered in this paper. Note that white Gaussian noise works appropriately only for sufficiently high temperatures. Analysis of Eqs. (6)- (9) reveals that the orthogonal ac-drive components $E_x(t)$ and $E_y(t)$ are nonlinearly coupled through the relativistic energy dispersion, leading to significant rectification induced by the periodic ratchet potential $V(x)$. The above mentioned equations describe the dynamics of a particle under the influence of driving forces and potential of a substrate which include effective parameters containing \hbar . Moreover, in these dynamical equations, x and y are real-space variables, whereas k_x and k_y are the x - and y - components, respectively, of the crystal momentum which can also be regarded as expectation values of their respective operators. It has been shown that two harmonic drives with commensurate frequencies can induce rectification, leading to direct current in the non-relativistic regime when both are applied along the same direction [49–51]. Remarkably, in the relativistic Langevin equations in Eqs. (6)- (9), coupling between the x and y degrees of freedom generates an unusual harmonic mixing, where rectification of current occurs even if the two harmonic drives are orthogonal to each other. Moreover, the damping coefficient η takes into account contributions from all possible collision mechanisms a charge carrier may undergo when moving through a twisted bilayer graphene sheet. Furthermore, the noisy environment in TBG can be provided by external noise sources such as current or voltage fluctuations. As a consequence, the interaction of a single charge carrier with such an environment generates damping effects, which are included in relativistic Langevin equations. The appropriate form of the damping and the fluctuating terms can be determined by the fluctuation-dissipation theorem.

III. RESULTS AND DISCUSSION

In this section, we present the results based on our semi-classical approach for describing Brownian dynamics of Dirac fermions in twisted bilayer graphene. It is illustrated that all simulations involved in the solution of Eqs. (6)- (9) have been performed employing the stochastic Runge-Kutta algorithm [52].

A. Relativistic ratchet effect

In this section, we consider charge carrier dynamics in the presence of rectification of non-equilibrium perturbations on a substrate with periodic ratchet potential $V(x)$. Here, we consider the driving electric field as

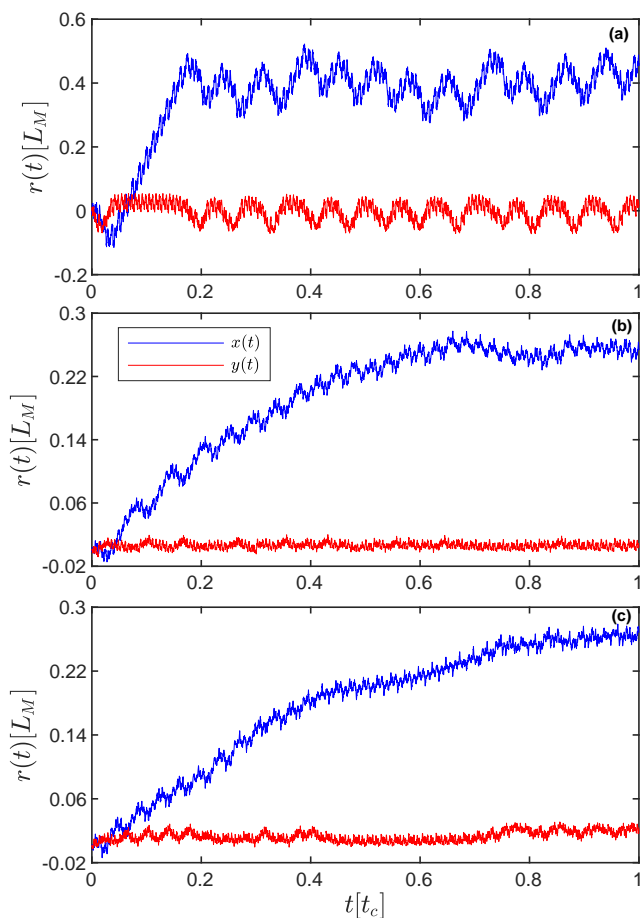


Figure 1. Real space trajectories of Brownian dynamics in twisted bilayer graphene for the twist angles: (a) $\theta = 1.03^\circ$, (b) $\theta = 1.05^\circ$, and (c) $\theta = 1.06^\circ$ in units of L_M for $\theta = 1.05^\circ$. The blue curve shows the x -component and the red curve is used for the y -component of the dynamics. The parameters used are: $t_c = \frac{\hbar}{W}$, $\omega_x = \omega_0$ with $\omega_0 = W/\hbar$, $\omega_y = 4\omega_x$, $eE_x = F_0$ with $F_0 = W/a$, $eE_y = 8eE_x$, $\eta = 0.03F_0/v_F$ with $v_F = Wa/\hbar$, $L = 700a$, $k_B T = 0.001W$, $V_0 = 120W$.

$$\mathbf{E}(t) = (E_x \cos(\omega_x t), E_y \cos(\omega_y t)), \text{ where } E_x \text{ and } E_y$$

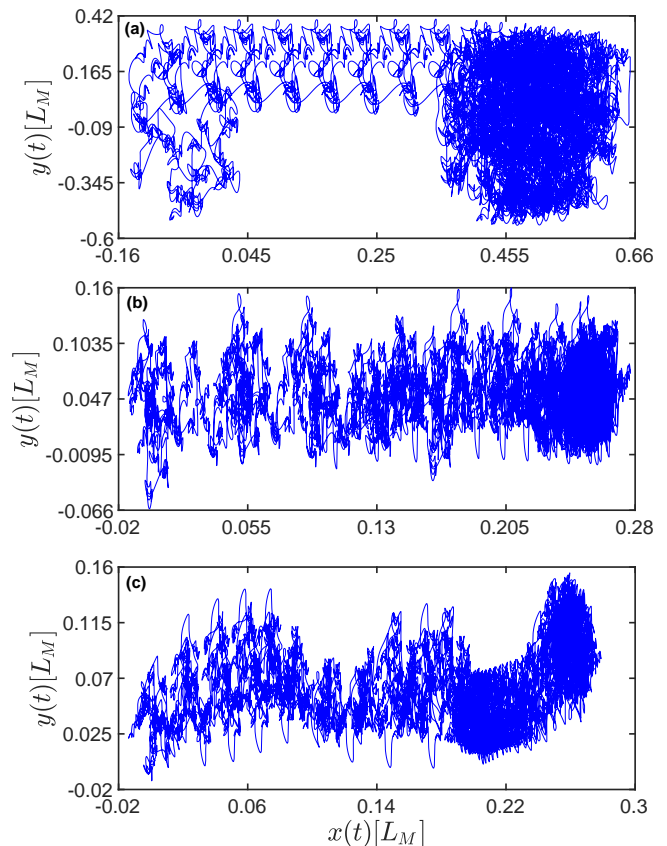


Figure 2. Real space trajectories of Brownian dynamics in twisted bilayer graphene for the twist angle: (a) $\theta = 1.03^\circ$, (b) $\theta = 1.05^\circ$, and (c) $\theta = 1.06^\circ$ in units of L_M for $\theta = 1.05^\circ$ in the xy -plane using the same parameters as used for Fig. 1.

are the amplitudes, ω_x and ω_y are the oscillation frequencies of the x - and y -components of the field. It has been shown that in the non-relativistic regime, ratcheting takes place only in the x -direction, induced by the periodic driving field, $E_x(t)$ oriented along x -axis. The rectification weakens if $\mathbf{E}(t)$ is rotated at an angle with the x -axis, until it drops to zero for ac drives parallel to the substrate valleys. In this process, the component $E_y(t)$ of the ac-field keeps the system out of equilibrium, however, it cannot be rectified, as the substrate potential is uniform in the y direction. Hence, the x and y dynamics remain decoupled. In the relativistic Langevin equations, see Eqs. (6)- (9), instead, the orthogonal ac-drive components, $E_x(t)$ and $E_y(t)$, are nonlinearly coupled through the relativistic dispersion relation, see Eq. (3), so that both can be rectified by the periodic ratchet potential $V(x)$. In order to understand the diffusion mechanism in twisted bilayer graphene, we analyze the real space trajectories of the driven Brownian dynamics. In Fig. 1, the real-space trajectories of the mentioned dynamics have been shown for different values of the twist angle. Comparison of panels (a), (b), and (c) reveals that the Brownian dynamics changes significantly with the change of twist angle. In particular, the trajectories of Brownian

particle for twist angle, $\theta = 1.03^\circ$ are significantly different from those plotted for $\theta = 1.05^\circ$ and $\theta = 1.06^\circ$, showing that the dynamics in TBG strongly depends on the twist angle and the randomness is more prominent for $0 < \theta < 1.05^\circ$. Moreover, comparison of the blue and red curves shows that the x - and y -components of Brownian dynamics exhibit different dynamical behavior. In Fig. 2, the real-space trajectories of Brownian particle have been shown for different values of the twist angle in the xy -plane. This figure also shows that the trajectories of Brownian particle exhibit irregular behavior. The characteristic feature of Brownian dynamics in TBG stems from the fact that the trajectories fall in the experimentally accessible regime that can be measured using the recently developed experimental techniques [53, 54]. Such trajectories have also been investigated in various systems [55, 56]. However, the amplitudes of trajectories in TBG are an order of magnitude larger than these systems. Analysis of Figs. 1 and 2 reflects random behavior of the particle dynamics, hallmark of Brownian dynamics. For further analysis and understanding the dynamics, we analyze the diffusion coefficient and net current in the following sections.

1. Diffusion coefficient

The Brownian particle described by the dynamical equations in Eqs. (6)- (9) drifts with average speed $\langle \dot{\mathbf{r}} \rangle$ in the direction of the applied resultant force, the random switches between locked and running states lead to a spatial dispersion of the particle around its average position. In the long-time limit, the corresponding effective diffusion coefficient can be expressed as [32]

$$D := \lim_{t \rightarrow \infty} \frac{\langle \mathbf{r}^2(t) \rangle - \langle \mathbf{r}(t) \rangle^2}{2t}, \quad (12)$$

where the two brackets denote average evaluated over the initial conditions of position and over all realizations of thermal noise and $\mathbf{r} = (x, y)$ are the x - and y -components of the trajectory. Fig. 3 shows the temperature dependence of diffusion coefficient in TBG for different values of the twist angle. This figure shows that the diffusion coefficient exhibits resonancelike behavior, where maximal is observed around $k_B T \sim 0.65W$, revealing the existence of an optimal $k_B T$ for the enhancement of diffusion rate. This mechanism is reminiscent of stochastic resonance [57–59]. The diffusion coefficient tends to minimal in the limits $T \rightarrow 0$ and $T \rightarrow \infty$, indicating the crucial role of thermal noise in the Brownian dynamics. The maximum in the diffusion coefficient can be understood by realizing that high temperature Jüttner distribution endows the relativistic particle an effective mass $m_{\text{eff}} = \frac{k_B T}{v_F^2}$, leading to a drop in diffusion at high temperature [32, 44]. Moreover, comparison of the blue solid, red asteric solid, green dash-dotted, and black dashed curves shows that the diffusion coefficient is minimal for

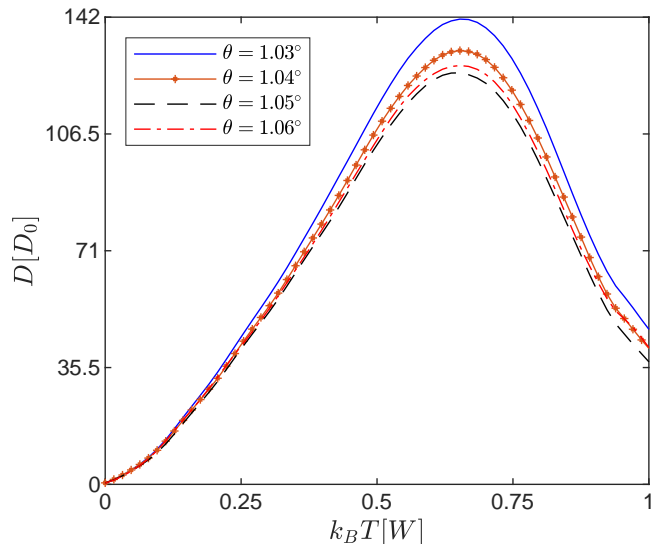


Figure 3. Diffusion coefficient D in units of $D_0 = \frac{k_B T}{\eta}$ versus thermal noise strength $k_B T$. The blue solid curve shows the diffusion coefficient for $\theta = 1.03^\circ$, the red asteric solid curve is used for $\theta = 1.04^\circ$, the black dashed curve is used for $\theta = 1.05^\circ$, and the green dash-dotted curve characterizes the diffusion coefficient for $\theta = 1.06^\circ$. The parameters used in numerical simulations are: $\omega_x = \omega_0$, $\omega_y = 4\omega_x$, $eE_x = F_0$, $eE_y = 7eE_x$, $\eta = 0.0001F_0/v_F$, $L = 700a$.

the twist angle that matches the magic angle ($\theta = 1.05^\circ$) where the band structure is flat [4, 15], corresponding to minimum velocity of the particle and consequently the diffusion rate is minimal. Hence, large diffusion is observed for $0 < \theta < 1.05^\circ$. Hence this mechanism appears in the presence of combined action of thermal noise, spatially varying periodic ratchet potential, and time-periodic modulating force fields. For simplicity and

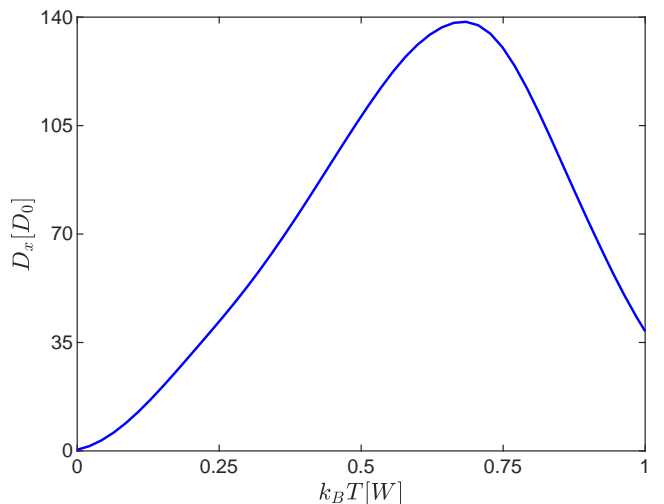


Figure 4. Diffusion coefficient D_x versus thermal noise strength $k_B T$ using $\theta = 1.05^\circ$ and $eE_x = 0$ using the same parameters as used in Fig. 3.

better understanding, we analyze the diffusion in one dimension, i.e., x -direction and ac drive forcing the charge carriers along y with $\mathbf{E}(t) = (0, E_y \cos(\omega_y t))$. By numerically solving the semiclassical relativistic Langevin equations, see Eqs. (6)-(9), one can observe that a relativistic particle tends to drift in the x -direction with net current and diffusion coefficient. More insight is obtained by plotting diffusion coefficient D_x as a function of thermal noise strength $k_B T$ using $\theta = 1.05^\circ$ as shown in Fig. 4. This figure shows that diffusion coefficient is maximal around $k_B T \approx 0.65W$. It is shown that a rectification is induced by $E_y(t)$ in the x -direction at finite temperature. The particle fluctuations are enhanced in the x -direction under the influence of thermal noise around the minima of periodic ratchet potential $V(x)$; as k_y is driven by $E_y(t)$ toward values on the order of \sqrt{T} , leading to maximize the velocity v_x and the Brownian particle is kicked in the x -direction, either to the right or to the left; this is how spatial asymmetry comes into play. Interestingly, such a rectification mechanism becomes ineffective when the particle sits at a potential minimum with $k_x = 0$, which only occurs in the absence of thermal noise, i.e., $T = 0$.

Moreover, the diffusion of Brownian particle also de-

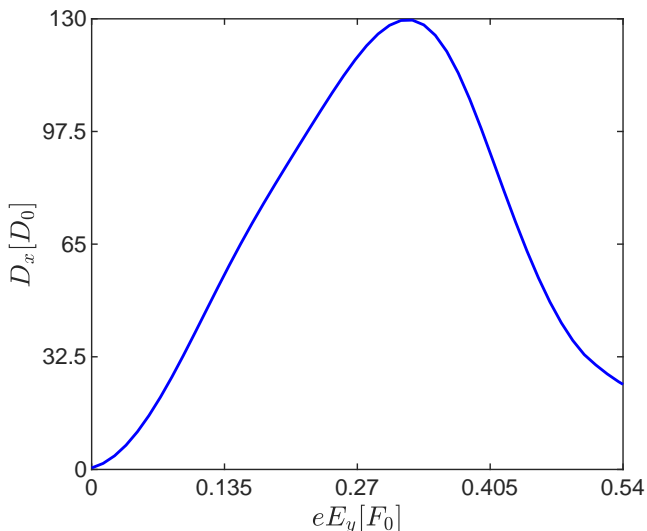


Figure 5. Diffusion coefficient D_x versus driving field strength eE_y using the same parameters as used for Fig. 3.

pends strongly on the amplitude of the driving force. To demonstrate this effect, the diffusion coefficient D_x is plotted as a function of driving force amplitude eE_y in Fig. 5. This figure shows that the diffusion coefficient is maximal around $eE_y \approx 0.3F_0$, where deterministically running solutions of the relativistic Langevin equations occur. Interesting feature in Fig. 5 is the resonancelike behavior of the diffusion coefficient around an optimal eE_y for the enhancement of the diffusion rate.

It is known that there are two states of a driven Brownian dynamics: locked state, in which the particle stays

inside one potential well that occurs in the regime of a small driving force strength, and the running state, in which the particle runs over the potential barriers which takes place when the amplitude of the external field is large where both diffusive and regular behavior of the particle dynamics can be observed. In these regions, the optimal matching of the periodic force and thermal noise drives the charge carriers up the potential hills during each time period. In turn these particles undergo scattering at the potential barriers and finally diffuse rapidly into the wide regions. It implies that an enhanced diffusion rate is obtained under the optimal collective actions of the spatial periodic potential, time periodic modulation, and stochastic stimulation.

Furthermore, the diffusion of Brownian particle is af-

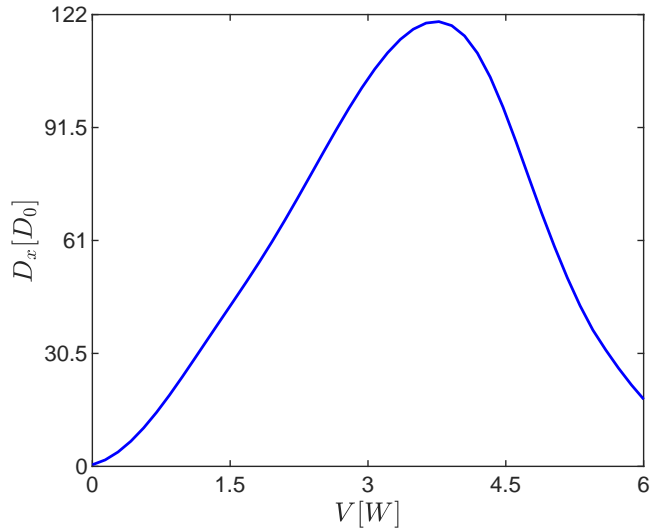


Figure 6. Diffusion coefficient D_x versus periodic ratchet potential strength V using the same parameters as used for Fig. 3.

ected significantly by changing strength of the ratchet potential of the substrate. To realize this effect, the diffusion coefficient is plotted as a function of ratchet potential strength in Fig. 6, showing that the diffusion coefficient is maximal around $V \approx 3.7W$. The interesting feature of Fig. 6 is the appearance of resonancelike behavior of the diffusion coefficient around the optimal ratchet potential strength. It mimics the behavior of the diffusion coefficient as a function of thermal noise shown in Fig. 4. If the potential wells are sufficiently deep relative to thermal noise i.e. V relative to $k_B T$ then diffusion is suppressed as seen in Fig. 6.

Further understanding of the diffusion mechanism in twisted bilayer graphene is obtained by analyzing the diffusion coefficient versus twist angle as shown in Fig. 7. It shows that the diffusion coefficient increases with the increase of twist angle, hits maximum at $\theta \approx 1.03^\circ$ and then decreases rapidly to become minimal. Hence, it is maximal around the twist angle, $\theta \approx 1.03^\circ$ which is in agreement with the appearance of large diffusion coeffi-

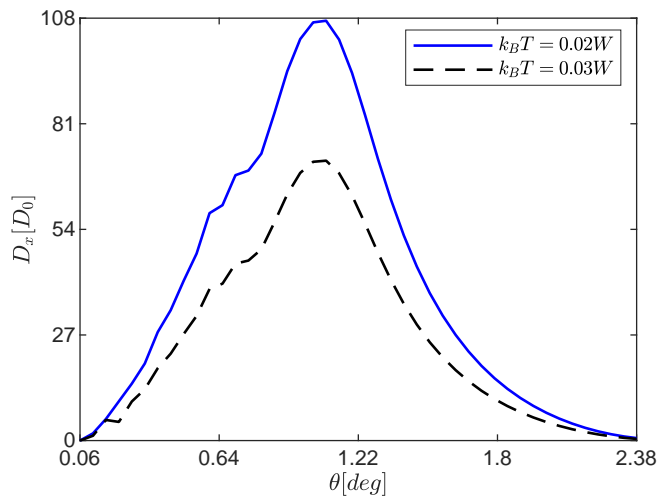


Figure 7. Diffusion coefficient D_x versus periodic ratchet potential strength V using the same parameters as used for Fig. 3.

cient for $\theta = 1.03^\circ$ in Fig. 3 and is minimal in the regions, $\theta \ll 1.03^\circ$ and $\theta \gg 1.03^\circ$, illustrating the key role of noise in the Brownian dynamics. This behavior of the diffusion coefficient indicates the existence of an optimal twist angle where the diffusion is maximal. Moreover, comparison of the blue solid and black dashed curves shows that diffusion coefficient decreases with increase of thermal energy of the system. Interestingly, Fig. 7 also shows that diffusion coefficient exhibits resonancelike behavior around the value of twist angle that matches the optimal angle.

2. Net current

In this section, we consider charge carrier transport in the presence of rectification of non-equilibrium perturbations on a substrate with periodic ratchet potential $V(x)$. It is shown that for a nonrelativistic particle under the influence of two force fields, the x and y components of position vector become statistically uncorrelated, resulting into vanishing average currents in both directions. However, for a relativistic particle the coupling between k_x and k_y leads to mixing the orthogonal components of ac electric field \mathbf{E} , producing a net current. Hence drifting of a relativistic particle generates net current given by

$$J = \frac{\langle \dot{\mathbf{r}} \rangle}{L}. \quad (13)$$

Eq. (13) reveals dependence of the net current on both the driving frequency and temperature of the system. The temperature dependence of this current is plotted in Fig. 8 for different values of the twist angle. It is evident from inspection of this figure that the current initially increases with increasing temperature, becomes maximal

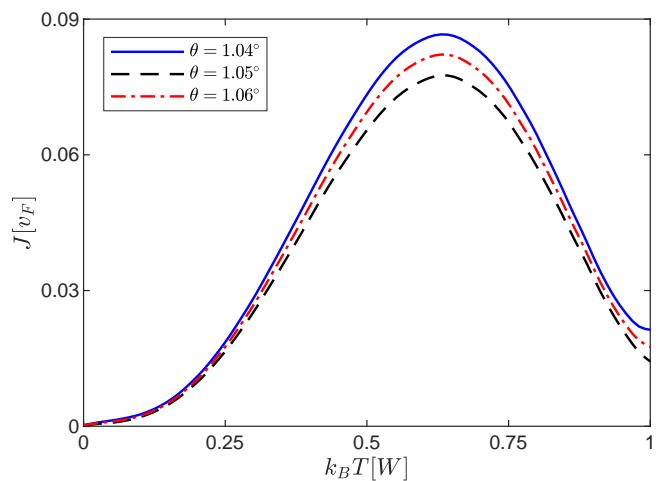


Figure 8. Diffusion coefficient D_x versus periodic ratchet potential strength V using the same parameters as used for Fig. 3.

around $0.65W$ and then decreases. This behavior of the net current illustrates the significant role played by noise in the Brownian dynamics. Comparison of the blue solid, red dash-dotted, and black dashed curves shows that the net current in twisted bilayer graphene depends strongly on the twist angle, where the net current is minimal for the magic angle, $\theta = 1.05^\circ$ which is in agreement with the results for diffusion coefficient in Fig. 3.

It is shown that the results of the present study are significantly different from the previous studies [44, 60, 61] due to the use of totally different model, encoding completely different effects and the underlying mechanism in this study. In particular, our results are different from the results of Ref. [44]. In the present work, the relativistic ratcheting depends strongly on the twist angle which is not relevant to monolayer graphene. In addition, we have analyzed the trajectories of Brownian particle and diffusion coefficient as a function of ratchet potential strength, driving field amplitude, and twist angle which are missing in the aforementioned paper. Moreover, the resonancelike behaviors of the diffusion coefficient and net current in twisted bilayer graphene are well pronounced compared to monolayer graphene. This difference appears due to the peculiar band structure of TBG that can be tuned through the twist angle that in turn affects significantly the dynamics of charge carriers in the system, presenting different scenario from monolayer graphene.

Finally, we propose experimental measurement of the Brownian dynamics of Dirac fermions in TBG using the recently developed experimental techniques [53, 54, 62, 63].

IV. CONCLUSIONS

In summary, Brownian dynamics of Dirac fermions in twisted bilayer graphene under the influence of orthogonal, commensurate ac drives in a periodic ratchet potential of a substrate has been investigated, illustrating key role of the twist angle. We have found that the real space trajectories are changed significantly by changing the twist angle. The diffusion coefficient exhibits resonancelike behavior around the optimal thermal noise strength, i.e., $k_B T \sim 0.65W$, where diffusion rate is maximal. The diffusion coefficient tends to minimal in the limits $T \rightarrow 0$ and $T \rightarrow \infty$, indicating the crucial role of thermal noise in the Brownian dynamics. Similar behaviors are exhibited by the diffusion coefficient as a function of ratchet potential strength and driving force field amplitude. It has been shown that the diffusion coefficient is minimal for twist angle that matches the magic angle ($\theta = 1.05^\circ$), whereas large diffusion coefficient is observed for $0 < \theta < 1.05^\circ$. Moreover, we have shown that the Dirac fermions in TBG exhibit remarkable ratchet effect as a net current. Analysis reveals that the net current initially increases with increase in temperature, becomes maximal and then decreases rapidly, illustrating the significant role played by thermal noise in the dynamics. As a consequence, as threshold parameter matches its optimal value, deterministic running states appear in the driven Brownian dynamics in the limit of weak thermal noise where the diffusion enhances signif-

icantly compared to bare thermal diffusion. We expect experimental measurement of the Brownian motion of Dirac fermions in TBG using the recently developed experimental techniques [53, 54, 62, 63].

Finally, it is illustrated that the findings of this work can be utilized in realizing electronic devices based on graphene cutting edge technologies.

ACKNOWLEDGMENTS

The author cordially acknowledges the support of Higher Education Commission (HEC), Pakistan under National Research Program for Universities NRP/PU Project No. 11459.

DATA AVAILABILITY STATEMENT

Data sharing is not applicable to this article, as it describes entirely theoretical research work.

DECLARATION OF COMPETING INTEREST

The author declares that he has no known competing financial interests or personal relationships that could have appeared to influence the work reported in this paper.

-
- [1] Y. Cao *et al.*, *Nature* **556**, 80 (2018).
 - [2] Y. Cao *et al.*, *Nature* **556**, 43 (2018).
 - [3] M. Yankowitz *et al.*, *Science* **363**, 1059 (2019).
 - [4] M. Koshino *et al.*, *Phys. Rev. X* **8**, 031087 (2018).
 - [5] G. Tarnopolsky, A. J. Kruchkov, and A. Vishwanath, *Phys. Rev. Lett.* **122**, 106405 (2019).
 - [6] J. Liu, J. Liu, and X. Dai, *Phys. Rev. B* **99**, 155415 (2019).
 - [7] Z. Song *et al.*, *Phys. Rev. Lett.* **123**, 036401 (2019).
 - [8] J. Kang and O. Vafek, *Phys. Rev. X* **8**, 031088 (2018).
 - [9] H. C. Po, L. Zou, A. Vishwanath, and T. Senthil, *Phys. Rev. X* **8**, 031089 (2018).
 - [10] G. Li *et al.*, *Nat. Phys.* **6**, 109 (2010).
 - [11] G. T. de Laissardi re, D. Mayou, and L. Magaud, *Nano Lett.* **10**, 804 (2010).
 - [12] A. Luican *et al.*, *Phys. Rev. Lett.* **106**, 126802 (2011).
 - [13] D. Wong *et al.*, *Phys. Rev. B* **92**, 155409 (2015).
 - [14] D. Wong *et al.*, *Proc. Natl. Acad. Sci. U.S.A.* **114**, 3364 (2017).
 - [15] R. Bistritzer and A. H. MacDonald, *Proc. Natl. Acad. Sci. U.S.A.* **108**, 12233 (2011).
 - [16] S. Fang and E. Kaxiras, *Phys. Rev. B* **93**, 235153 (2016).
 - [17] J. M. B. Lopes dos Santos, N. M. R. Peres, and A. H. Castro Neto, *Phys. Rev. Lett.* **99**, 256802 (2007).
 - [18] P. San-Jose, J. Gonz alez, and F. Guinea, *Phys. Rev. Lett.* **108**, 216802 (2012).
 - [19] E. J. Mele, *Phys. Rev. B* **81**, 161405(R) (2010).
 - [20] M. He *et al.*, *Nat. Phys.* **17**, 26 (2021).
 - [21] P. A. Pantale on, T. Low, and F. Guinea, *Phys. Rev. B* **103**, 205403 (2021).
 - [22] C.-P. Zhang *et al.*, *Phys. Rev. B* **106**, L041111 (2022).
 - [23] N. Tilak *et al.*, *Nat. Commun.* **12**, 4180 (2021).
 - [24] X. Lu, B. Lian, G. Chaudhary and D. K. Efetov, *Proc. Natl. Acad. Sci. U.S.A.* **118**, e2100006118 (2021).
 - [25] A. Kerelsky *et al.*, *Nature* **572**, 95 (2019).
 - [26] Y. Xie *et al.*, *Nature* **572**, 101 (2019).
 - [27] Y. Jiang *et al.*, *Nature* **573**, 91 (2019).
 - [28] Y. Choi *et al.*, *Nat. Phys.* **15**, 1174 (2019).
 - [29] S. L. Tomarken *et al.*, *Phys. Rev. Lett.* **123**, 046601 (2019).
 - [30] M. I. B. Utama *et al.*, *Nat. Phys.* **17**, 184 (2020).
 - [31] S. Lisi *et al.*, *Nat. Phys.* **17**, 189 (2020).
 - [32] P. H anggi and F. Marchesoni, *Rev. Mod. Phys.* **81**, 387 (2009).
 - [33] A. J. Friedman, R. Vasseur, A. Lamacraft, and S. A. Parameswaran, *Phys. Rev. B* **100**, 060301(R) (2019).
 - [34] C. L. Vestergaard, P. C. Blainey, and H. Flyvbjerg, *Phys. Rev. E* **89**, 022726 (2014).
 - [35] A. Pototsky and F. Marchesoni, *Phys. Rev. E* **87**, 32132 (2013).
 - [36] M. Serag and S. Habuchi, *Nat. Commun.* **8**, 15675 (2017).
 - [37] I. Santra, U. Basu, and S. Sabhapandit, *Phys. Rev. E* **104**, L012601 (2021).
 - [38] Z. A. Hajaj and M. Z. Saghir, *Processes* **9**, 1965 (2021).

- [39] J. Mo and M. G. Raizen, *Annu. Rev. Fluid Mech.* **51**, 403 (2019).
- [40] F. J. Martín-Pasquín and A. N. Pisarchik, *Mathematics* **9**, 2503 (2021).
- [41] D. Boyanovsky and D. Jasnow, *Phys. Rev. A* **96**, 062108 (2017).
- [42] E. Cobanera, P. Kristel, and C. Morais Smith, *Phys. Rev. B* **93**, 245422 (2016).
- [43] C. Lewandowski and L. Levitov, *Proc. Natl. Acad. Sci. U.S.A.* **116**, 20869 (2019).
- [44] A. Pototsky, F. Marchesoni, F. V. Kusmartsev, P. Hänggi and S. E. Savelév, *Eur. Phys. J. B* **85**, 356 (2012).
- [45] J.-F. Derivaux, R. L. Jack, and M. E. Cates, *J. Stat. Mech.*, 043203 (2022).
- [46] P. Reimann, M. Grifoni, and P. Hänggi, *Phys. Rev. Lett.* **79**, 10 (1997).
- [47] J. Dunkel and P. Hänggi, *Phys. Rep.* **471**, 1 (2009).
- [48] M. Müller, J. Schmalian, and L. Fritz, *Phys. Rev. Lett.* **103**, 025301 (2009).
- [49] F. Marchesoni, *Phys. Lett. A* **119**, 221 (1986).
- [50] S. Savelév, F. Marchesoni, P. Hänggi, F. Nori, *Europhys. Lett.* **67**, 179 (2004).
- [51] S. Savelév, F. Marchesoni, P. Hänggi, F. Nori, *Eur. Phys. J. B* **40**, 403 (2004).
- [52] Rebecca L. Honeycutt, *Phys. Rev. A* **45**, 600 (1992).
- [53] S. Kheifets, A. Simha, K. Melin, T. Li, M. G. Raizen, *Science* **343**, 1493 (2014).
- [54] O. F. Petrov, K. B. Statsenko and M. M. Vasiliev, *Sci. Rep.* **12**, 8618 (2022).
- [55] L. Ma, X. Li, and C. Liu, *J. Chem. Phys.* **145**, 114102 (2016).
- [56] M. Evstigneev and A. Al-Haidari, *J. Phys. A: Math. Theor.* **52**, 055001 (2019).
- [57] P. Hänggi, P. Talkner, and M. Borkovec, *Rev. Mod. Phys.* **62**, 251 (1990).
- [58] R. Benzi, A. Sutera, and A. Vulpiani, *J. Phys. A: Math. Gen.* **14**, 453 (1981).
- [59] L. Gammaitoni, F. Marchesoni, E. Menichella-Saetta, and S. Santucci, *Phys. Rev. Lett.* **62**, 349 (1989).
- [60] P. Reimann *et al.*, *Phys. Rev. E* **65**, 031104 (2002).
- [61] M. Bandyopadhyay, S. Dattagupta, and M. Sanyal, *Phys. Rev. E* **73**, 051108 (2006).
- [62] A. Tamtögl *et al.*, *Nat. Commun.* **11**, 278 (2020).
- [63] M. Grimm, T. Franosch, and S. Jeney, *Phys. Rev. E* **86**, 021912 (2012).